MATERIALS SCIENCE

Excited state engineering for efficient reverse intersystem crossing

Hiroki Noda[1], Hajime Nakanotani[1,2,3]*, Chihaya Adachi[1,2,3]*

Reverse intersystem crossing (RISC) from the triplet to singlet excited state is an attractive route to harvesting electrically generated triplet excitons as light, leading to highly efficient organic light-emitting diodes (OLEDs). An ideal electroluminescence efficiency of 100% can be achieved using RISC, but device lifetime and suppression of efficiency roll-off still need further improvement. We establish molecular design rules to enhance not only the RISC rate constant but also operational stability under electrical excitation. We show that the introduction of a second type of electron-donating unit in an initially donor-acceptor system induces effective mixing between charge transfer and locally excited triplet states, resulting in acceleration of the RISC rate while maintaining high photoluminescence quantum yield. OLEDs using our designed sky-blue emitter achieved a nearly 100% exciton production efficiency and exhibited not only low efficiency roll-off but also a marked improvement in operational stability.

INTRODUCTION

Organic light-emitting diodes (OLEDs), which can reach internal electroluminescence (EL) quantum efficiencies (IQEs) of nearly 100%, are one of the most promising devices for next-generation displays and lighting. According to spin statics (*1*), 75% of excitons are directly generated in the triplet excited state (T) after carrier recombination, so two approaches exist to obtain an ideal IQE: phosphorescence (*2*, *3*), in which triplet excitons directly produce EL, and thermally activated delayed fluorescence (TADF) (*4*), in which reverse intersystem crossing (RISC) of triplet excitons to the singlet excited state (S) results in delayed fluorescence (DF). In particular, since molecules exhibiting TADF can be designed without using expensive rare-metal elements such as iridium, the number of reports on molecular design for TADF has significantly increased (*5*), resulting in an abundance of emitter molecules achieving an ideal IQE (*6*–*8*). However, an investigation not only of the RISC mechanism itself, but also of the relationship between the rate constant of RISC (k_{RISC}) and molecular design, which is a critical issue for the development of high-performance, commercially viable TADF-OLEDs, especially with blue emission, is still needed.

Reduction of exciton density (n_S for singlet and n_T for triplet) in the device during electrical excitation is a key consideration for improving operational stability in TADF-OLEDs (*9*, *10*). In particular, high n_T induces detrimental exciton annihilation and/or chemical reactions because of the long exciton lifetime of triplets (*11*, *12*). Thus, the k_{RISC} should be maximized. The basic strategy for increasing k_{RISC} in aromatic compounds is by reducing the energy splitting between the lowest S (S_1) and lowest T (T_1), that is, ΔE_{ST}, because the first-order coefficient for mixing between two states is inversely proportional to ΔE_{ST} (*13*). In addition, the influence of not only ΔE_{ST} but also second-order spin-vibronic coupling between charge transfer (CT) and locally excited (LE) triplet states on the RISC process has been proposed by several groups recently (*14*–*19*). These theoretical and experimental conclusions indicate that the mixing of wave functions between CT and LE is an important factor for accelerating RISC in molecules. However, there is still no clear strategy for molecular design to realize maximum TADF performance based on these principles. Another important consideration is the charge transport abilities of the molecules inside the emissive layer (EML). Since a narrow carrier recombination zone in the EML induces a high n_S and n_T, the carrier recombination zone should be spread as much as possible (*20*, *21*).

Here, we propose a molecular design to establish both (i) effective mixing of the wave function between CT and LE excited states and (ii) tuning of charge transport ability by the introduction of a second electron-donating unit in an initially donor (D)–acceptor (A) system. Our designed molecule exhibits a k_{RISC} that is one order of magnitude larger than that of the template molecule while maintaining a high photoluminescence quantum yield (PLQY). Furthermore, TADF-OLEDs using the molecule as emitter exhibit not only a remarkable enhancement of operational stability but also suppression of exciton annihilation processes with an external EL quantum efficiency (EQE) of more than 20% even in the high luminance region.

RESULTS

Our molecular design strategy for ideal TADF performance requires the following four conditions. (i) The organic molecule should have a D-A system to form intramolecular CT states, which provide a small ΔE_{ST} according to spatial separation of the highest occupied molecular orbital (HOMO) and the lowest unoccupied molecular orbital (LUMO). (ii) The molecule should have two or more D units to form a delocalized CT triplet state ($^3CT^{de}$) (*18*), which provides a stable T state. (iii) The conformational change between S and T should be suppressed to achieve high device stability; thus, a sterically crowded molecule is preferred. (iv) Finally, since electron transition between a pure triplet CT state (^3CT) and a pure singlet CT state (^1CT) is forbidden because of a vanishing of the spin-orbit coupling matrix elements between these molecular orbitals, the mediation of a molecular orbital with character other than CT, such as an LE state, is required to open a route for RISC, which can be enhanced by the mixing of LE character to an excited state wave function of ^3CT, that is, a small energy gap between ^3LE and ^3CT ($\Delta E_{^3LE-{}^3CT}$).

In this contribution, 5CzBN, which has five carbazole (Cz) units and one benzonitrile (BN) unit, was used as a template molecule (Fig. 1A) (*22*). BN is well known to be a strong electron-accepting unit with a high $^3LE_1$ of 3.32 eV (*23*). On the other hand, phenyl-Cz (PhCz) is

[1]Center for Organic Photonics and Electronics Research (OPERA), Kyushu University, 744 Motooka, Nishi, Fukuoka 819-0395, Japan. [2]International Institute for Carbon Neutral Energy Research, Kyushu University, Nishi, Fukuoka 819-0395, Japan. [3]Japan Science and Technology Agency, Exploratory Research for Advanced Technology, Adachi Molecular Exciton Engineering Project, c/o OPERA, Kyushu University, Nishi, Fukuoka 819-0395, Japan.
*Corresponding author. Email: nakanotani@cstf.kyushu-u.ac.jp (H.N.); adachi@cstf.kyushu-u.ac.jp (C.A.)

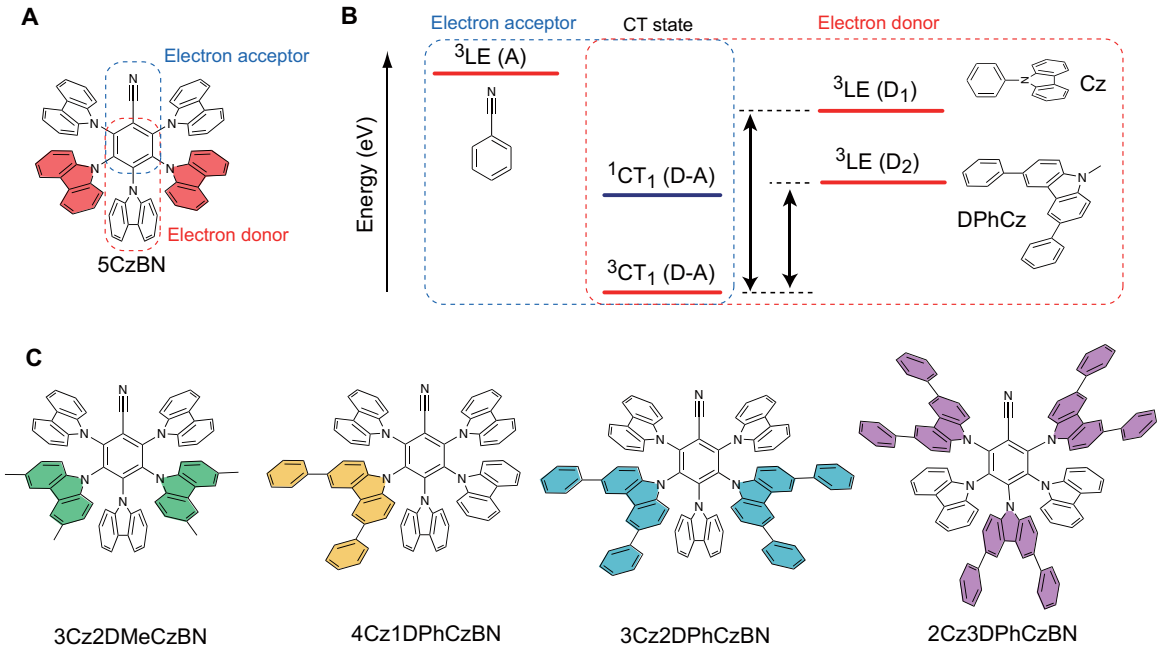

Fig. 1. Excited state energy level alignment for RISC. (**A**) Chemical structure of 5CzBN. (**B**) Schematic illustration of $^1CT_1$, $^3CT_1$, and $^3LE_1$ energy level alignment for RISC. (**C**) Chemical structure of D-D_2-A–type CzBN derivatives. The second type of substituted donor units is highlighted in the chemical structures.

often used as a D unit, especially in blue TADF emitters because PhCz also has a high $^3LE_1$ of 3.10 eV. Therefore, the combination of these D and A units in 5CzBN leads to the effective transfer of an excited electron on the Cz to BN, resulting in the formation of $^1CT_1$ (2.94 eV) and $^3CT_1$ (2.77 eV). While Hosokai *et al.* (*24*) already reported that the T_1 state of 5CzBN has CT character, we also confirmed the solvatochromism of the phosphorescence spectra of 5CzBN (fig. S2), indicating that the T_1 state of 5CzBN has more CT character than LE character despite the vibronic phosphorescence spectra. In addition, transient absorption spectroscopy experimentally confirmed the presence of a radical Cz cation in the triplet excited state of 5CzBN (*18*), indicating again the formation of a CT state in the triplet excited state. However, we cannot explain the origin of the vibronic spectrum of the phosphorescence in toluene at this stage. Since the molecular structure of 5CzBN is rigid and dense, one possible reason for the origin of the vibronic spectrum of the phosphorescence is the suppression of molecular vibrations at 77 K. Since the $^3LE_1$ energies of Cz and BN are much higher than the $^3CT_1$ energy of 5CzBN, the triplet energy of $^3CT_1$ is sufficiently confined, resulting in a molecule that shows TADF activity. However, the energy gap between $^3LE_1$ of Cz and $^3CT_1$ ($\Delta E_{^3LE-^3CT}$ = 0.32 eV) is much larger than ΔE_{ST} (0.17 eV). Therefore, 5CzBN does not sufficiently satisfy condition (iv), not only because of the weak mixing between ^3LE and ^3CT but also because of the endothermic positioning of $^3LE_1$ relative to $^1CT_1$.

To satisfy condition (iv), we propose the introduction of a second type of donor (D_2) unit having a lower $^3LE_1$ than that of PhCz while maintaining the original Cz-BN–based CT system (Fig. 1B). To maintain the original D-A CT system, we mainly introduce the D_2 into the *m*-position of BN because the *o*- and *p*-positions of BN show high electron-donating properties. Figure 1C shows the chemical structures of our designed molecules. Since substitution of aromatic or methyl groups in the 3,6-position of Cz is expected to lower the $^3LE_1$ energy, we used 3,6-diphenylcarbazole (DPhCz) and 3,6-dimethylcarbazole (DMeCz) as D_2. These compounds were easily synthesized via a nucleophilic substitution reaction with good reaction yields of more than 80%. Although 5CzBN showed a low solubility [<0.1 weight % (wt %)] in toluene, we obtained a good solubility of more than 0.1 wt % for 3Cz2DPhCzBN even with its higher molecular weight (MW = 1232.46) than 5CzBN (MW = 928.33). This is likely due to a reduction of molecular symmetry, and this improved solubility can enable easier purification of the compounds and the possibility of fabricating OLEDs by solution processing.

First, to confirm whether the type of D_2 has an effect on the RISC process, we compared PL characteristics of 5CzBN, 3Cz2DMeCzBN, and 3Cz2DPhCzBN. Although the fluorescence spectra of 3Cz2DMeCzBN and 3Cz2DPhCzBN were slightly red-shifted, the emission was still sky blue with a peak wavelength of 480 nm, as shown in Fig. 2A. Further, modification of the initial D-A system by D_2 had no effect on ΔE_{ST} (0.15–0.17 eV) in 5CzBN (*18*), 3Cz3DMeCzBN, and 3Cz2DPhCzBN, which was confirmed experimentally by the difference in onset energies of fluorescence and phosphorescence in diluted toluene solutions (fig. S1). Thus, these compounds might be expected to exhibit similar TADF properties. However, as summarized in Table 1, these compounds show notable differences.

All of the compounds exhibited similar radiative decay rate constants (k_r) of 1.3×10^7 to 2.5×10^7 s^{-1} for singlets and a marked increase in PLQY attributed to DF after degassing by bubbling with argon (Table 1), indicating that the triplet excitons efficiently convert to singlet excitons through RISC and then emit DF. On the other hand, the DF lifetime (τ_d) greatly decreased with the introduction of D_2, resulting in a faster τ_d of 12.0 μs for 3Cz2DPhCzBN than for 5CzBN (46.8 μs), as shown in Fig. 2B. Because of the reduction of τ_d while maintaining a high PLQY, 3Cz2DPhCzBN has a k_{RISC} (7.2×10^5 s^{-1}) that is more than three times larger than that of 5CzBN. To assess the RISC processes in these compounds in more detail, we measured the temperature dependence of k_{RISC}. From an Arrhenius plot of the k_{RISC}, we estimated activation

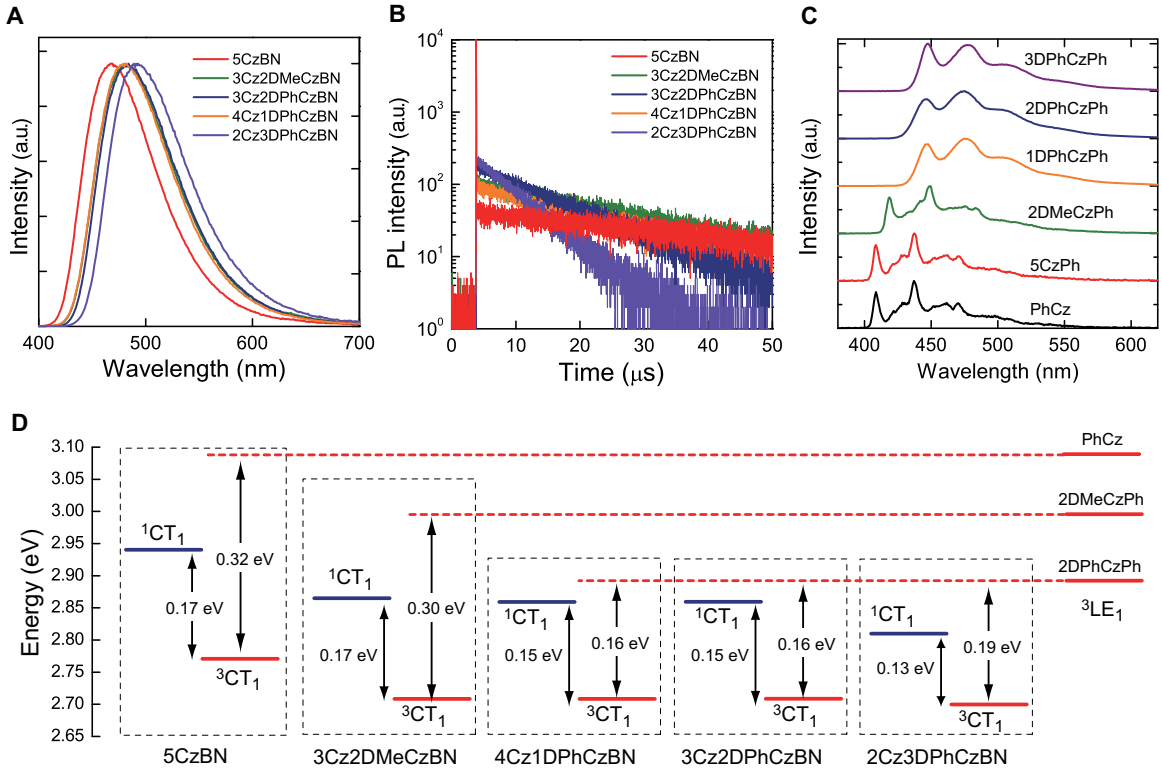

Fig. 2. Photoluminescence properties of D-D_2-A–type molecules. (**A**) Steady-state fluorescence spectrum for each molecule in toluene at 295 K. a.u., arbitrary units. (**B**) PL transient decay curves of CzBN derivatives in oxygen-free toluene at 295 K. (**C**) Phosphorescence spectra of CzPh, 5CzPh, 2DMeCzPh, 1DPhCzPh, 2DPhCzPh, and 3DPhCzPh in oxygen-free toluene at 77 K. (**D**) Energy level diagram of CzBN derivatives. The dashed red lines indicate the $^3LE_1$ of CzPh for reference.

Table 1. Photophysical characteristics of CzBN derivatives in toluene

Compound	PL_{max} (nm)	PLQY (%)*	ΔE_{ST} (eV)†	$\Delta E_{^3LE-^3CT}$ (eV)‡	$\Delta E_{^1CT-^3LE}$ (eV)§	E_a (eV)¶	τ_p (ns)	τ_d (μs)	k_r (10^7 s^{-1})	k_{ISC} (10^8 s^{-1})	k_{RISC} (10^5 s^{-1})	k_{nrT} (10^4 s^{-1})
5CzBN	470	7/75	0.17	0.32	−0.10	0.13	3.8	46.8	1.9	2.5	2.2	0.6
3Cz2DMeCzBN	480	8/85	0.17	0.30	−0.13	0.10	5.9	23.6	1.3	1.5	4.4	0.7
4Cz1DPhCzBN	480	11/85	0.15	0.16	−0.01	0.09	7.0	19.4	1.6	1.3	3.9	0.9
3Cz2DPhCzBN	480	9/81	0.15	0.16	−0.01	0.06	5.8	12.2	1.5	1.5	7.2	1.7
2Cz3DPhCzBN	492	13/83	0.13	0.19	−0.06	0.08	5.2	6.1	2.5	1.7	10.2	3.2

*PLQY for before (left) and after (right) Ar bubbling. The error is ±2%. †Energy gap between S_1 and T_1 states. The error is ±0.03 eV. ‡Energy gap between $^3CT_1$ and $^3LE_1$ states. The error is ±0.03 eV. §Energy gap between $^1CT_1$ and $^3LE_1$ states. The error is ±0.03 eV. ¶The error is ±0.01 eV.

energies for RISC (E_a) to be 0.13, 0.10, and 0.06 eV for 5CzBN, 3Cz2DMeBN, and 3Cz2DPhCzBN, respectively (fig. S3), indicating a reduction of E_a that is independent of ΔE_{ST}. We also note that the nonradiative decay rate constant (k_{nr}^T) for T of 5CzBN ($k_{nr}^T = 0.6 \times 10^4$ s^{-1}) was smaller than that of 3Cz2DPhCzBN, so the suppression of k_{nr}^T is not responsible for the faster τ_d.

Next, to check the effect of the number of D_2 units, we designed 4Cz1DPhCzBN and 2Cz3DPhCzBN, which have one and three D_2 units of DPhCz, respectively. The fluorescence and phosphorescence spectra and PLQY of 4Cz1DPhCzBN nearly match those of 3Cz2DPhCzBN; thus, these compounds might also be expected to have similar ΔE_{ST}. However, we observed a smaller k_{RISC} of 3.9×10^5 s^{-1} for 4Cz1DPhCzBN, leading to a slightly larger E_a of 0.09 eV. On the other hand, 2Cz3DPhCzBN has a k_{RISC} (1.0×10^6 s^{-1}) that is one order of magnitude higher than that of 5CzBN, but its emission spectrum is markedly red-shifted compared to that of 5CzBN. This red shift indicates that the DPhCz unit acts as the primary donor rather than D_2, which is a result of the DPhCz units substituted in *o*- and *p*-positions of BN, leading to CT formation between DPhCz and BN units.

To understand the increase of k_{RISC} without a reduction of ΔE_{ST}, we examined the $^3LE_1$ of D_2 in these compounds because the A unit remained constant. Figure 2C shows the phosphorescence spectra of

PhCz, 5CzPh, 2DMeCzPh, 3DPhCzPh, 2DPhCzPh, and 1DPhCzPh. The phosphorescence spectrum of 5CzPh closely resembles that of PhCz, indicating that the $^3LE_1$ of 5CzPh is from PhCz. This case is specific to TADF molecules using Cz as a donor moiety. For example, in the case of a diphenylamine donor moiety, which is also widely used in TADF molecules, increasing the number of diphenylamine units leads to a lower triplet energy, as shown in fig. S4. On the other hand, the $^3LE_1$ energies of 2DMeCzPh (2.99 eV) and 2DPhCzPh (2.87 eV) are noticeably lower than that of 5CzPh (3.10 eV), leading to a reduction of $\Delta E_{^3LE-{}^3CT}$, as shown in Fig. 2D. Thus, by introduction of 2DMeCzPh and 2DPhCzPh as second donor units in 5CzBN, the ^3LE states could be controlled. These results provide experimental evidence not only of the possibility of tuning the energy level of the $^3LE_1$ state by introducing a second type of donor into a D-A system but also of the strong influence of the energy level alignment of $^3LE_1$, $^3CT_1$, and $^1CT_1$, that is, $\Delta E_{^3LE-{}^3CT}$ and $\Delta E_{^1CT-{}^3LE}$, on RISC. Although we cannot completely exclude the presence of unknown triplet excited states between $^3LE_1$ of the donor moiety and $^3CT_1$ of the compound, the decrease of the ^3LE state of the donor moiety should cause mixing between LE and CT character naturally when the donor and acceptor moieties are combined, leading to acceleration of k_{RISC}. Thus, by introduction of a second donor, mixing between the ^3LE state and other triplet states will be increased because of the reduction of the energy level of the ^3LE state.

Although $^3LE_1$ exhibits no dependency on the number of DPhCz units in Fig. 2C, k_{RISC} changes with the number of D_2 units. Since second-order spin-vibronic coupling is related to the term $|\langle^1\Psi_{CT}|H_{SOC}|^3\Psi_{LE}\rangle\langle^3\Psi_{LE}|H_{vib}|^3\Psi_{CT}\rangle|^2$ (*14*), increasing the number of D_2 units increases the probability for vibronic coupling between the ^3LE and ^3CT states by increasing the electron density of D_2 units, thereby effectively inducing RISC through second-order spin-vibronic coupling. The phosphorescence lifetime of 3Cz2DPhCzBN (120 ms) was appreciably shorter than that of 4Cz1DPhCzBN (136 ms) or 5CzBN (138 ms), indicating the strong mixing between S and T via second-order spin-vibronic coupling. These experimental results provide us with a clear molecular design rule for accelerating RISC: Minimize $\Delta E_{^3LE-{}^3CT}$ in addition to ΔE_{ST}, which can be done by introducing an appropriate number of a second type of donor units with a suitable donating ability. In addition, we note that these findings also have consequences for the choice of a host-guest matrix for TADF emitters. Since $^3LE_1$ influences the RISC process, organic molecules that have triplet energies higher than not only $^3CT_1$ but also $^3LE_1$ of the TADF emitter are favorable as the host matrix to suppress back-energy transfer from $^3LE_1$ of the TADF emitter to a triplet state of the host matrix.

To demonstrate the impact of an increased k_{RISC} on OLED performance, we fabricated OLEDs with 5CzBN or 3Cz2DPhCzBN:mCBP [3,3-di(9*H*-carbazol-9-yl)biphenyl] codeposited films as EML. The photophysical properties of 3Cz2DPhCzBN are almost the same as those of 5CzBN, with the only difference being in terms of k_{RISC}. Therefore, we investigated the OLED properties with 5CzBN or 3Cz2DPhCzBN as emitters. Figure S3 shows schematic diagrams of the energy levels of the fabricated devices and the chemical structures of the organic semiconductor materials used in them (*25*). Here, we note that 20 wt %–doped codeposited films showed PLQYs of 65 ± 2% and 80 ± 2% for 5CzBN and 3Cz2DPhCzBN, respectively (Table 2).

The characteristics of the fabricated OLEDs are shown in Fig. 3 (A to D) and summarized in Table 3. The EL spectrum of each device was red-shifted compared with that of the emitter in solution because of the relatively high doping concentration of the emitters, but the EL emission color coordinates still correspond to bluish-green emission. Figure 3B shows the EQE luminance characteristics of the tested OLEDs. The OLEDs exhibited a high EQE at 500 cd m^{-2} of 18.0% for 5CzBN and 20.9% for 3Cz2DPhCzBN. However, as shown in the inset of Fig. 3C, the EQE roll-off characteristics differ. Although EQE quickly drops to 94 and 77% of its maximum value at 1000 and 5000 cd m^{-2}, respectively, in the OLED based on 5CzBN, EQE roll-off was suppressed in the OLED based on 3Cz2DPhCzBN, which maintained 99.5 and 89% of the maximum EQE at 1000 and 5000 cd m^{-2}, respectively. A trend of suppressed EQE roll-off with higher k_{RISC} is apparent (see also fig. S4), suggesting that exciton annihilation processes such as triplet-singlet and triplet-triplet annihilation are suppressed in the EML through a reduction of triplet exciton density because of a higher k_{RISC} (*10*, *11*). Since high brightness is required for practical applications such as lighting, the weak EQE roll-off even at a high-luminance region is a valuable advantage.

Next, we assessed the operational stability of the fabricated OLEDs. Figure 3C shows the normalized luminance of the two representative OLEDs as a function of operational time under constant current density at an initial luminance L_0 of 1000 cd m^{-2}. Although a rapid decrease of luminance with increasing operation time was observed in the 5CzBN-based OLED, for which the time until the luminance decreased to 97% of the initial (LT97) was only 3 hours, we observed a marked enhancement of operational stability in the 3Cz2DPhCzBN-based OLED, resulting in an LT97 of more than 100 hours.

Since such a large lifetime enhancement cannot be explained only by the increase of k_{RISC}, we suspect that a shifting of the carrier recombination zone in the EMLs plays a role. Although the HOMO (−6.1 eV for both) and LUMO (−3.3 eV for 5CzBN and −3.4 eV for 3Cz2DPhCzBN) levels of both molecules are almost the same, the driving voltage of the 3Cz2DPhCzBN-based OLED was slightly higher than that of the 5CzBN device (Fig. 3D). To check the carrier transport abilities of both EMLs, we analyzed the current density (*J*)–voltage (*V*) characteristics in electron-only devices (EODs) and hole-only devices (HODs) based on emitter:mCBP codeposited films (the device structures are presented in the caption of fig. S5). We found a reduction of electron current in the 3Cz2DPhCzBN-based EOD compared to the 5CzBN device while the

Table 2. Photophysical characteristics of 20 wt %–doped mCBP films

Compound	PL_{max} (nm)	PLQY (%)*	τ_p (ns)	τ_d (μs)	k_r (10^7 s^{-1})	k_{ISC} (10^8 s^{-1})	k_{RISC} (10^5 s^{-1})	k_{nrT} (10^4 s^{-1})
5CzBN	486	16/65	3.2	10.2	5.0	2.6	3.6	4.1
3Cz2DPhCzBN	495	14/80	4.5	5.65	3.0	1.9	9.9	4.1

*PLQY for prompt (left) and delayed (right) component. The error is ±2%.

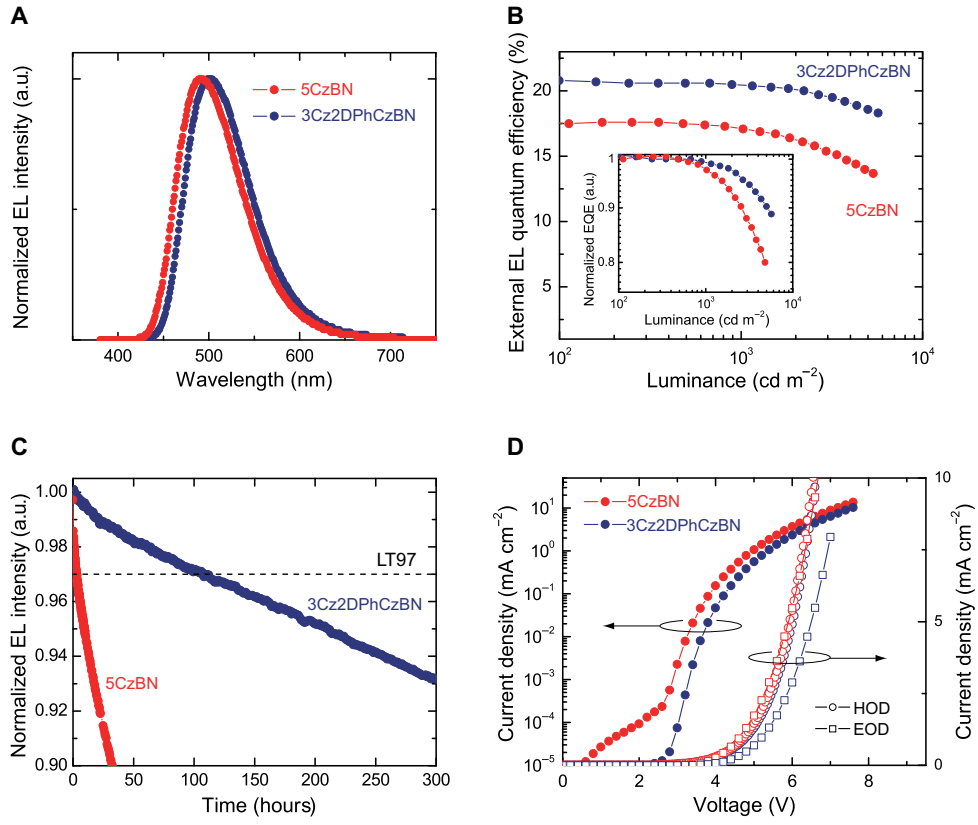

Fig. 3. Device performance of OLEDs. (**A**) EL spectrum in the OLEDs at 100 cd m^{-2}. (**B**) EQE in the OLEDs as a function of luminance. Inset: Normalized EQE characteristics in the OLEDs. (**C**) Normalized luminance of the OLEDs as a function of operating time at a constant current density. The initial luminance was 1000 cd m^{-2} for each OLED, corresponding to constant driving current density at 2.4 and 1.6 mA cm^{-2} for 5CzBN- and 3Cz2DPhCzBN-based OLEDs, respectively. (**D**) Current density–voltage characteristics for OLEDs (filled circles), EODs (open squares), and HODs (open circles) based on 5CzBN or 3Cz2DPhCzBN as dopant.

Table 3. Device performance of OLEDs based on CzBN emitters

Emitter	Voltage (V)*	EQE (%)*	Current efficiency (cd A^{-1})*	CIE (chromaticity coordinates)	LT97 (hours)†
5CzBN	5.0/5.6/7.7	18.0/17.0/13.9	44.9/43.6/35.0	(0.19, 0.41)	3
3Cz2DPhCzBN	5.2/5.8/7.4	20.9/20.8/18.6	63.0/62.2/55.9	(0.21, 0.44)	110

*Voltage, EQE, and current efficiency were obtained at 500, 1000, and 5000 cd m^{-2}, respectively. The error for EQE is ±0.2%, which was obtained from at least four devices. †Initial luminance of 1000 cd m^{-2}.

hole currents were similar (Fig. 3D), indicating that the introduction of a bulky substituent might be preventing carrier transport because of weaker molecular interactions between neighboring molecules. Since the HOMO level of the guest is similar to that of the mCBP host, injected holes are expected to be mainly transported through the HOMO level of mCBP, resulting in the choice of guest having no effect on the hole current. Reduced electron transport in the 3Cz2DPhCzBN-based OLED can be expected to result in an expansion of carrier recombination zone inside the EML because the carrier recombination zone is located near the electron blocking layer/EML interface in the 5CzBN-based OLED (see fig. S5), leading to the reduction of the n_T in the device during electrical excitation (*21*). In addition, Zhang *et al.* (*22*) reported that operational stability increases by introducing the substitution in Cz units such as a *tert*-butyl unit according to the enhancement of electrochemical stability. Thus, we strongly believe that the marked enhancement of operational lifetime in the 3Cz2DPhCzBN-based OLED originates from a combination of an increase in k_{RISC}, an expansion of the carrier recombination zone, and the contribution of the substitution effect of Cz units.

DISCUSSION

We found that introduction of a second type of donor (D_2) into a D-A system can be used to tune the energy position of $^3LE_1$ relative to $^1CT_1$ and $^3CT_1$ while, at the same time, weakly pinning the $^1CT_1$ and $^3CT_1$ energy levels to those of the original D-A system, resulting in an increase of k_{RISC} according to a strong second-order spin-vibronic coupling between $^3LE_1$ and $^3CT_1$. In addition, the $^3LE_1$ can be adjusted by changing the number or donor ability of the D_2 units. Further, we also found that the carrier transport properties in the EML can be tuned by the use of a bulky substituent, resulting in a change in the position and width of the carrier recombination zone. Thus, our molecular design rule and strategy are useful for boosting OLED performance, especially for blue TADF emitters, and will aid the development of future displays and lighting with high EL efficiencies and long operational lifetimes.

MATERIALS AND METHODS

Synthesis and characterization

2,3,4,5,6-Penta(9*H*-carbazol-9-yl)benzonitrile (5CzBN), 2,4,6-tris(9*H*-carbazol-9-yl)-3,5-difluorobenzonitrile (3CzFBN), 2,3,4,6-tetrakis(9*H*-carbazol-9-yl)-5-fluorobenzonitrile (4CzFBN), and 3,6,9-triphenylcarbazole (1DPhCzPh) were synthesized according to literature (*26*–*28*). CzBN derivatives, 5CzPh, 2DPhCzPh, 2DMeCzPh, and 3DPhCzPh were synthesized and characterized according to the methods described in section S1.

Measurement of photoluminescence properties

PL quantum efficiency was measured under the flow of argon gas using an absolute PL quantum yield measurement system (C11347-01, Hamamatsu Photonics) with an excitation wavelength of 340 nm. Emission lifetimes were measured using a fluorescence lifetime measurement system (C11367-03 Quantaurus-Tau, Hamamatsu Photonics) and CoolSpek Cs-0296 (UNISOKU Co.). Ultraviolet-visible (UV-vis) absorption spectra and PL spectra were recorded on UV-vis (Lambda 950-PKA, PerkinElmer) and PL (FluoroMax-4, HORIBA Jobin Yvon) spectrophotometers. Phosphorescence spectra in solution at 77 K were recorded on a Hamamatsu Photonics multichannel analyzer (PMA-12).

Device fabrication and characterization of OLED performance

Glass substrates with a prepatterned, 50- or 100-nm-thick, tin-doped indium oxide coating were used as anodes. Organic layers were formed by thermal evaporation. Doped EMLs were deposited by coevaporation. After device fabrication, devices were immediately encapsulated with glass lids using epoxy glue in a nitrogen-filled glove box [$O_2 < 0.1$ parts per million (ppm); $H_2O < 0.1$ ppm]. Commercial calcium oxide desiccant (Dynic Co.) was included in each encapsulated package. The current density–voltage–luminance characteristics of the OLEDs were evaluated using a source meter (Keithley 2400, Keithley Instruments Inc.) and an absolute external quantum efficiency measurement system (C9920-12, Hamamatsu Photonics). The operational lifetime was measured using a luminance meter (SR-3AR, TOPCON) with the devices operated at a constant DC current. All measurements were performed in ambient atmosphere at room temperature.

SUPPLEMENTARY MATERIALS

Supplementary material for this article is available at http://advances.sciencemag.org/cgi/content/full/4/6/eaao6910/DC1

Synthesis and characterization of CzBN derivatives, 5CzPh, 2DPhCzPh, 2DMeCzPh, and 3DPhCzPh.

fig. S1. Fluorescence and phosphorescence spectra of the CzBN derivatives.

fig. S2. Phosphorescence spectra of 5CzBN in toluene and acetonitrile solutions.

fig. S3. Arrhenius plots of the k_{RISC} for CzBN derivatives.

fig. S4. Phosphorescence spectra of triphenylamine and 1,4-bis(diphenylamino)benzene in toluene solutions.

fig. S5. Chemical structure and energy diagram of TADF-OLED devices.

fig. S6. EQE as a function of luminance for 5CzBN, 3Cz2DMeCzBN, and 3Cz2DPhCzBN.

fig. S7. EQE–current density in the OLEDs with 5CzBN as emitter.

fig. S8. ^1H and ^{13}C nuclear magnetic resonance (NMR) spectra of 3Cz2DPhCzBN.

fig. S9. ^1H and ^{13}C NMR spectra of 3Cz2DMeCzBN.

fig. S10. ^1H and ^{13}C NMR spectra of 4Cz1DPhCzBN.

fig. S11. ^1H and ^{13}C NMR spectra of 2F3DPhCzBN.

fig. S12. ^1H and ^{13}C NMR spectra of 2Cz3DPhCzBN.

fig. S13. ^1H and ^{13}C NMR spectra of 5CzPh.

fig. S14. ^1H and ^{13}C NMR spectra of 2DPhCzPh.

fig. S15. ^1H and ^{13}C NMR spectra of 3DMeCzPh.

fig. S16. ^1H and ^{13}C NMR spectra of 3DPhCzPh.

REFERENCES AND NOTES

1. M. A. Baldo, D. F. O'Brien, M. E. Thompson, S. R. Forrest, Excitonic singlet-triplet ratio in a semiconducting organic thin film. *Phys. Rev. B* **60**, 14422–14428 (1999).
2. M. A. Baldo, D. F. O'Brien, Y. You, A. Shoustikov, S. Sibley, M. E. Thompson, S. R. Forrest, Highly efficient phosphorescent emission from organic electroluminescent devices. *Nature* **395**, 151–154 (1998).
3. S. Reineke, F. Lindner, G. Schwartz, N. Seidler, K. Walzer, B. Lüssem, K. Leo, White organic light-emitting diodes with fluorescent tube efficiency. *Nature* **459**, 234–238 (2009).
4. A. Endo, M. Ogasawara, A. Takahashi, D. Yokoyama, Y. Kato, C. Adachi, Thermally activated delayed fluorescence from Sn^{4+}–porphyrin complexes and their application to organic light emitting diodes—A novel mechanism for electroluminescence. *Adv. Mater.* **21**, 4802–4806 (2009).
5. M. Y. Wong, E. Zysman-Colman, Purely organic thermally activated delayed fluorescence materials for organic light-emitting diodes. *Adv. Mater.* **29**, 1605444 (2017).
6. H. Uoyama, K. Goushi, K. Shizu, H. Nomura, C. Adachi, Highly efficient organic light-emitting diodes from delayed fluorescence. *Nature* **492**, 234–238 (2012).
7. S. Hirata, Y. Sakai, K. Masui, H. Tanaka, S. Y. Lee, H. Nomura, N. Nakamura, M. Yasumatsu, H. Nakanotani, Q. Zhang, K. Shizu, H. Miyazaki, C. Adachi, Highly efficient blue electroluminescence based on thermally activated delayed fluorescence. *Nat. Mater.* **14**, 330–336 (2015).
8. T.-A. Lin, T. Chatterjee, W.-L. Tsai, W.-L. Lee, M.-J. Wu, M. Jiao, K.-C. Pan, C.-L. Yi, C.-L. Chung, K.-T. Wong, C.-C. Wu, Sky-blue organic light emitting diode with 37% external quantum efficiency using thermally activated delayed fluorescence from spiroacridine-triazine hybrid. *Adv. Mater.* **28**, 6976–6983 (2016).
9. H. Nakanotani, T. Higuchi, T. Furukawa, K. Masui, K. Morimoto, M. Numata, H. Tanaka, Y. Sagara, T. Yasuda, C. Adachi, High-efficiency organic light-emitting diodes with fluorescent emitters. *Nat. Commun.* **5**, 4016–4023 (2014).
10. T. Furukawa, H. Nakanotani, M. Inoue, C. Adachi, Dual enhancement of electroluminescence efficiency and operational stability by rapid upconversion of triplet excitons in OLEDs. *Sci. Rep.* **5**, 8429 (2015).
11. K. Masui, H. Nakanotani, C. Adachi, Analysis of exciton annihilation in high-efficiency sky-blue organic light-emitting diodes with thermally activated delayed fluorescence. *Org. Electron.* **14**, 2721–2726 (2013).
12. S. Schmidbauer, A. Hohenleutner, B. König, Chemical degradation in organic light-emitting devices: Mechanisms and implications for the design of new materials. *Adv. Mater.* **25**, 2114–2129 (2013).
13. N. J. Turro, V. Ramamurthy, J. C. Scaiano, Quantum dynamics: Transitions between states, in *Principle of Molecular Photochemistry: An Introduction* (University Science Books, 2009), chap. 3, pp. 113–118.
14. X.-K. Chen, S.-F. Zhang, J.-X. Fan, A.-M. Ren, Nature of highly efficient thermally activated delayed fluorescence in organic light-emitting diode emitters: Nonadiabatic effect between excited states. *J. Phys. Chem. C* **119**, 9728–9733 (2015).
15. J. Gibson, A. P. Monkman, T. J. Penfold, The importance of vibronic coupling for efficient reverse intersystem crossing in thermally activated delayed fluorescence molecules. *ChemPhysChem* **17**, 2956–2961 (2016).
16. F. B. Dias, J. Santos, D. R. Graves, P. Data, R. S. Nobuyasu, M. A. Fox, A. S. Batsanov, T. Palmeira, M. N. Berberan-Santos, M. R. Bryce, A. P. Monkman, The role of local triplet excited states and D-A relative orientation in thermally activated delayed fluorescence: Photophysics and devices. *Adv. Sci.* **12**, 1600080 (2016).
17. C. M. Marian, Mechanism of the triplet-to-singlet upconversion in the assistant dopant ACRXTN. *J. Phys. Chem. C* **120**, 3715–3721 (2016).
18. T. Hosokai, H. Matsuzaki, H. Nakanotani, K. Tokumaru, T. Tsutsui, A. Furube, K. Nasu, H. Nomura, M. Yahiro, C. Adachi, Evidence and mechanism of efficient thermally activated delayed fluorescence promoted by delocalized excited states. *Sci. Adv.* **3**, e1603282 (2017).
19. J. Gibson, T. J. Penfold, Nonadiabatic coupling reduces the activation energy in thermally activated delayed fluorescence. *Phys. Chem. Chem. Phys.* **19**, 8248–8434 (2017).
20. N. C. Erickson, R. J. Holmes, Investigating the role of emissive layer architecture on the exciton recombination zone in organic light-emitting devices. *Adv. Mater.* **23**, 5190–5198 (2013).
21. Y. Zhang, J. Lee, S. R. Forrest, Tenfold increase in the lifetime of blue phosphorescent organic light-emitting diodes. *Nat. Commun.* **5**, 5008 (2014).
22. D. D. Zhang, M. Cai, Y. Zhang, D. Zhang, L. Duan, Sterically shielded blue thermally activated delayed fluorescence emitters with improved efficiency and stability. *Mater. Horiz.* **3**, 145–151 (2016).
23. K. Takei, Y. Kanda, Phosphorescence spectra of benzonitrile and related compounds. *Spectrochim. Acta* **18**, 1201–1216 (1962).
24. T. Hosokai, H. Noda, H. Nakanotani, T. Nawata, Y. Nakayama, H. Matsuzaki, C. Adachi, Solvent-dependent investigation of carbazole benzonitrile derivatives: Does the ^3LE–^1CT energy gap facilitate thermally activated delayed fluorescence? *J. Photonics Energy* **8**, 032102 (2018).

25. L.-S. Cui, S.-B. Ruan, F. Bencheikh, R. Nagata, L. Zhang, K. Inada, H. Nakanotani, L.-S. Liao, C. Adachi, Long-lived efficient delayed fluorescence organic light-emitting diodes using n-type hosts. *Nat. Commun.* **8**, 2250 (2017).
26. Y. J. Cho, S. K. Jeon, J. Y. Lee, Molecular engineering of high efficiency and long lifetime blue thermally activated delayed fluorescent emitters for vacuum and solution processed organic light-emitting diodes. *Adv. Opt. Mater.* **4**, 688–693 (2016).
27. Y. J. Cho, B. D. Chin, S. K. Jeon, J. Y. Lee, 20% external quantum efficiency in solution-processed blue thermally activated delayed fluorescent devices. *Adv. Funct. Mater.* **25**, 6786–6792 (2015).
28. M. Park, J. R. Buck, C. J. Rizzo, A convenient synthesis of 3,6-substituted carbazoles via nickel catalyzed cross-coupling. *Tetrahedron* **54**, 12707–12714 (1998).

Acknowledgments: We acknowledge W. J. Potscavage Jr. for his assistance with preparation of this manuscript. We also acknowledge helpful discussions with A. Endo, D. P.-K. Tsang, and N. Noutsuka. **Funding:** This work was supported in part by the Japan Science and Technology Agency, Exploratory Research for Advanced Technology, Adachi Molecular Exciton Engineering Project (grant number JPMJER1305). **Author contributions:** H. Nakanotani and H. Noda conceived and designed the project. H. Noda performed the synthetic work. H. Noda and H. Nakanotani determined photophysical properties and analyzed data. H. Noda fabricated devices, and H. Nakanotani and H. Noda analyzed the data. H. Nakanotani, H. Noda, and C.A. wrote the manuscript. C.A. supervised the project. All the authors discussed the results and contributed to the article. **Competing interests:** H. Nakanotani, H. Noda, and C.A. are inventors on a Japan patent application related to this work filed by Kyushu University (2017-91634, 2 May 2017). C.A. has a minor ownership interest in one of the sponsors of this work (Kyulux Inc.). The authors declare no other competing interests. **Data and materials availability:** All data needed to evaluate the conclusions in the paper are present in the paper and/or the Supplementary Materials. Additional data related to this paper may be requested from the authors.

Submitted 16 August 2017
Accepted 15 May 2018
Published 22 June 2018
10.1126/sciadv.aao6910

Citation: H. Noda, H. Nakanotani, C. Adachi, Excited state engineering for efficient reverse intersystem crossing. *Sci. Adv.* **4**, eaao6910 (2018).

Excited state engineering for efficient reverse intersystem crossing

Hiroki Noda, Hajime Nakanotani and Chihaya Adachi

Sci Adv **4** (6), eaao6910.
DOI: 10.1126/sciadv.aao6910